Accepted Manuscript

Strain rate sensitivities of deformation mechanisms in magnesium alloys

Huamiao Wang, Peidong Wu, Srihari Kurukuri, Michael J. Worswick, Yinghong Peng, Ding Tang, Dayong Li

PII: S0749-6419(17)30645-9

DOI: 10.1016/j.ijplas.2018.04.005

Reference: INTPLA 2333

To appear in: *International Journal of Plasticity*

Received Date: 11 November 2017

Revised Date: 5 April 2018

Accepted Date: 5 April 2018

Please cite this article as: Wang, H., Wu, P., Kurukuri, S., Worswick, M.J., Peng, Y., Tang, D., Li, D., Strain rate sensitivities of deformation mechanisms in magnesium alloys, *International Journal of Plasticity* (2018), doi: 10.1016/j.ijplas.2018.04.005.

Strain Rate Sensitivities of Deformation Mechanisms in Magnesium Alloys

- Huamiao Wang[a,b,c], Peidong Wu[b], Srihari Kurukuri[d], Michael J. Worswick[d], Yinghong Peng[a], Ding Tang[a], Dayong Li[a,c,*]

[a]State Key Laboratory of Mechanical Systems and Vibration, Shanghai Jiao Tong University, Shanghai, China, 200240

[b]Department of Mechanical Engineering, McMaster University, Hamilton, Ontario, Canada, L8S 4L7

[c]Materials Genome Initiative Center, Shanghai Jiao Tong University, Shanghai, China, 200240

[d]Department of Mechanical and Mechatronics Engineering, University of Waterloo, Waterloo, Ontario, Canada, N2L 3G1

Abstract:

Strain rate sensitivity (SRS) is an important material property that governs the rate dependent mechanical behaviors associated with deformation rate changes, creep, stress relaxation, formability, etc. The variety of activated deformation mechanisms of magnesium alloys under different loading paths, e.g. tension vs. compression, implies that SRS of magnesium alloys obviously depends on loading paths, and each deformation mechanism has its own SRSs. However, a single SRS scheme is commonly employed in numerical modeling to describe the rate dependent behaviors of magnesium alloys, which disregards the distinction of SRSs among different deformation mechanisms. The implementation of the constitutive model that works for a wide range of values of SRSs has been a challenge to crystal plasticity modeling for metals with multiple deformation mechanisms like magnesium. Especially, very small values of SRS, corresponding to low rate-sensitivity, generally lead to high nonlinearity involved in the governing equations, and then computational failure. In this paper, the elasto-viscoplastic self-consistent (EVPSC) crystal plasticity model is improved to enhance its numerical robustness for very small SRS values. Taking advantage of this improvement, different SRSs for various deformation mechanisms are employed to investigate the strain rate dependent behaviors of magnesium alloys at room temperature. First, the SRSs for various deformation mechanisms are determined based on the compressive stress relaxation tests on an AZ31 alloy plate; secondly, the obtained SRSs are applied to interpret internal elastic strain evolution of the same magnesium alloy under in-plane compression; finally, the determined SRSs are applied to investigate the deformation of another AZ31 alloy under various deformation paths and strain rates. The present work is the first effort on studying effects of strain rate-sensitivity on mechanical behavior of Mg alloys under wide range of applied strain rates by using an improved self-consistent polycrystal plasticity model. Good agreement between the experiments and simulations reveals the importance and necessity of using different SRSs for the deformation mechanisms involved. The rate dependent behaviors of magnesium alloys can be better described by using multiple SRSs associated to each operative deformation mechanism.

*Corresponding author: Dr. Dayong Li, dyli@sjtu.edu.cn, Tel.: +86-21-34206313

Keywords: Magnesium alloy; Strain rate sensitivity; Slip systems; Twinning; Crystal plasticity.

1. Introduction

Magnesium alloys have been gained great attention as potential materials to reduce the weight of vehicles in the past two decades. Their mechanical properties, such as flow stress, anisotropy, ductility and failure, etc., has been extensively studied. Strain rate sensitivity (SRS) of metals is another important property. The mechanical properties of a material are usually influenced by deformation rate due to strain rate sensitivity, and strain rate hardening can improve the formability of metals. Previous studies on cubic metals found that a single SRS could well describe their rate-dependent behaviors. For instance, the SRS of aluminum alloys is on the order of 0.001 (e.g., Wu et al., 1997), copper is approximately 0.0025 (Follansbee and Kocks, 1988), and stainless steel is around 0.016 at lower strain when phase transformation is unnoticeable (Talyan et al, 1998; Wang et al., 2013a). However, magnesium alloys show much more complicated rate-sensitive behaviors, corresponding to their complex deformation mechanisms. In addition to temperature (Karimi et al., 2013), alloying elements (Ang et al., 2017), SRS of magnesium alloys also exhibits obvious dependency on loading paths. For example, the term "compressive strain rate sensitivity" is used to describe the SRS of magnesium alloys under compression (Song et al., 2009). For magnesium alloys, multiple deformation mechanisms exist and play simultaneous but different roles under various loading paths, due to their hexagonal close packed crystallographic structure (Agnew and Duygulu, 2005, Wang et al., 2010a). The similar dependency on loading paths suggests that one deformation mechanism not only has its own SRS, but also has very different value from each another.

Several studies, mainly experimental, have examined the SRSs of the different deformation mechanisms active in magnesium alloys. The deformation mechanisms of magnesium alloys commonly active at room temperature are basal slip, prismatic slip, pyramidal slip and extension twinning (Agnew and Duygulu, 2005, Wang et al., 2010a). Magnesium alloy sheets were found to exhibit strong strain rate sensitivity during slip dominated deformation processes, e.g., in-plane tension, while show nearly strain rate insensitive during twin-dominated deformation processes, e.g., in-plane compression of magnesium alloy sheets (Khan et al., 2011; Karimi et al.,

2013; Kurukuri et al., 2014a; Kurukrui et al., 2014b; Xie et al., 2016; Ang et al., 2017; Habib et al., 2017; Li et al., 2017). In light of this, strain rate sensitivity measurements were used to identify twinning and changes in deformation mechanisms of an AZ31 alloy (Korla and Chokshi, 2010). Strain rate insensitivity and even negative strain rate sensitivity, though with very small absolute value (<0.01), were observed when deformation twinning is dominant in deformation (Chun and Davies, 2011). At higher imposed strains, the strain rate sensitivity is more significant corresponding to the multiple slip mechanisms activated. The strain rate sensitivity of basal slip dominated deformation of magnesium single crystal is found to be ~0.01 at room temperature (Bhattacharya and Niewczas, 2011). The influence of initial microstructure on the strain rate sensitivities of as-cast and wrought Mg-3Al-1Zn alloys at elevated temperature have been investigated (Beer and Barnett, 2006). Karimi et al. (2013) investigated the strain rate sensitivity of a wrought AZ31 magnesium alloy using the strain rate jump testing technique over a wide temperature range of 200°C ~500°C. The determined strain rate sensitivity at the low temperature ranges from 0 to 0.04 at different strain levels. Kurukuri et al. (2014) studied the strain rate sensitivity through tensile and compressive tests of AZ31B sheets at room temperature over the strain rate range from 0.001 to 1000 s^{-1}. Slip dominated deformation processes (in-plane tension and compression along ND) exhibited strong strain rate dependency, while twin-dominated deformation processes (in-plane compression) were found to be strain rate insensitive. Watanabe and Ishikawa (2009) have reported a low strain rate sensitivity of ~10^{-6} for basal slip and extension twin, and a strain rate sensitivity of ~0.02 for prismatic slip. Ulacia et al. (2010) have reported that the pyramidal slip has a strain rate sensitivity of ~0.01. Tang et al. (2015) and Wang et al. (2016a) have investigated stress relaxation in an AZ31 alloy through experiment. The amount of the stress drops during stress relaxation (constant strain) under in-plane compression increased significantly as a function of the imposed strain, due to occurrence of different deformation mechanisms at different strain levels. This observation also suggests different deformation mechanisms possess different strain rate sensitivities. In summary, deformation twinning exhibits almost rate-insensitive behaviour, basal slip exhibits low strain rate sensitivity, and prismatic slip and pyramidal slip present relatively higher rate sensitivity.

The previous experimental works indicate different deformation mechanisms have different SRSs for magnesium alloys. However, the quantitatively connection between the SRSs and the relevant behaviours of magnesium alloys has not been well established and therefore

need to be systematically investigated. In current work, based on the available experimental results, the rate-dependent behaviours of magnesium alloys are studied by the crystal plasticity modelling considering different SRSs for different deformation mechanisms. As for the modeling, macroscopic continuum models are not suitable because different SRSs for multiple deformation mechanisms cannot be implemented (García-Grajales et al., 2016). The often-used crystal plasticity models to describe the mechanical response of polycrystalline materials include crystal plasticity finite element (Dawson et al., 2000, 2001; Bronkhorst et al., 2007; Abdolvand et al., 2011; Wu et al., 2014; Qiao et al., 2015a), crystal plasticity-based Fast Fourier Transform (CP-FFT) models (Lebensohn et al., 2012) and mean-field effective-medium self-consistent (SC) models (Lebensohn and Tomé, 1993; Turner and Tomé, 1994; Wang et al., 2010c; 2016c; 2017). By accounting for the stress and strain heterogeneity inside a grain, CP-FE and CP-FFT are far more computationally expensive than the effective medium self-consistent (SC) polycrystal models. The latter treats the polycrystalline aggregate as a homogenous effective medium (HEM) with the average properties of the aggregate, and each grain as an ellipsoidal inclusion embedded in and interacting with the HEM. The computationally efficient SC polycrystal models are better suited to the current study since stress and strain heterogeneity inside a grain is not the interest. Among the SC polycrystal models, the elasto-plastic self-consistent (EPSC) model (Turner and Tomé, 1994) and the viscoplastic self-consistent (VPSC) model (Lebensohn and Tomé, 1993) are two popular models. However, the former cannot simulate rate-dependent problems since it ignores the strain rate sensitivity of materials. The latter cannot simulate the rate related stress relaxation problem since it ignores the elastic deformation. Instead, the elastic-visco-plastic self-consistent (EVPSC) model (Molinari, 1997; Wang et al., 2010c) is more suitable to study the strain rate sensitivity of a material because it accounts for both elasticity and rate relativity. The effects of stress relaxation and creep on the macroscopic stress-strain response and the internal elastic strain evolution within magnesium alloys were first studied numerically using the EVPSC model by Wang et al. (2012a). Later, these effects have been studied both experimentally using *in-situ* neutron diffraction and numerically with the EVPSC model for stainless steel (Wang et al., 2013a) and magnesium alloys (Wang et al., 2016a). It should be emphasized that a single set of EVPSC hardening parameters can address monotonic, stress relaxation and creep results of internal strain and macroscopic stress-strain evolution. The case of stress relaxation, is particularly challenging for polycrystal plasticity modelling, since elastic deformation, plastic

deformation and strain rate sensitivity are coupled together, whereas the EVPSC model has been shown to provide accurate predictions of the rate-dependent behaviors of materials (Wang et al., 2013a; 2016a). A physics-based crystal plasticity model for HCP crystals including both twinning and de-twinning (TDT), has been implemented into the finite strain EVPSC model for polycrystals (denoted as EVPSC-TDT) and successfully applied to study the twinning and de-twinning behavior of magnesium alloys (Wang et al., 2012b, Wang et al., 2013b, c; 2015a, b; 2016a, b; Qiao et al., 2015a). Therefore, the EVPSC-TDT model will be employed here to investigate the SRSs of various deformation mechanisms in magnesium alloys.

As for the treatment of SRS of multiple deformation mechanisms involved in magnesium alloys, most of the previous modeling works pre-assumed a single SRS (typically 0.05) for all deformation mechanisms (Proust et al., 2009; Wang et al., 2013b, c; Guo et al., 2013). In these cases, the strain rate effect might not be the primary research interest. One study modified the critical resolved shear stress (CRSS) of each deformation mechanism to address the strain rate effect of zirconium (Beyerlein and Tomé, 2008). In this case, the usage of SRS was only for computational convenience, not for the accurate determination of the material strain rate constitutive properties. It is of great interest to describe the rate-dependent behaviours of magnesium alloys in terms of strain rate sensitivities, which are easy to be understood and can be easily used in other applications. However, the implementation of the constitutive model that works for a wide range of values of SRSs has been a challenge to crystal plasticity modeling. Especially, very small values of SRS, corresponding to low rate-sensitivity, generally lead to high nonlinearity involved in the governing equations, and then computational failure. The available EVPSC and VPSC code did not work in this case because, as mentioned above, twinning in magnesium alloys has been found to be nearly rate-insensitive. An attempt has been made by Knezevic et al. (2016) to overcome the numerical difficulties associated with very low rate-sensitivity. They proposed a “k-mod” method and implemented it into the VPSC code, and then successfully simulate strain rate-sensitive deformation of Cu, which has a single slip family, from 10^{-4}/s to 10^{4}/s. On the other hand, the rate-sensitive behavior of plasticity originates from either dislocation nucleation and mobility at higher strain rates, or thermally-activated dislocation escape at lower strain rates (Zheng et al., 2016); the understanding the dependence of rate sensitivity on slip systems is of great interest (Movahedi-Rad and Alizadeh, 2017). The

molecular Dynamics Simulation of aluminum single crystal did show that SRS differs among different slip systems.

In the present work, the EVPSC-TDT model is improved to enhance its numerical robustness and allow for different/small SRSs for various deformation mechanisms. Then the improved model is applied to determine SRS values for various deformation mechanisms, and then interpret the stress relaxation test, lattice strain test and strain rate change tests. To the best of our knowledge, the present work is the first effort on studying effects of strain rate-sensitivity on mechanical behavior of magnesium alloys, which involves multiple and coupled deformation mechanisms, under wide range of applied strain rates by using a self-consistent polycrystal plasticity model. The article is organized as follows. In Section 2, the EVPSC model is briefly described. In Section 3, results and discussion are presented. Finally, conclusions are drawn in Section 4.

2. EVPSC-TDT model

A brief description of the twinning and de-twinning model is provided below. A more detailed description of the EVPSC-TDT model can be found elsewhere (Wang et al. 2010c; 2013b, c). The plastic shear rate associated with a deformation system α is (Asaro and Needleman, 1985):

$$\dot{\gamma}^{\alpha} = \dot{\gamma}_0 |\tau^{\alpha}/\tau_{cr}^{\alpha}|^{1/m^{\alpha}} sgn(\tau^{\alpha}) \quad (1)$$

where $\dot{\gamma}_0$ is a reference shear rate, τ_{cr}^{α} is the critical resolved shear stress (CRSS), and m^{α} is the strain rate sensitivity associated with the system α. In contrast to the previous works on crystal plasticity modeling of magnesium alloys, where a single value of $m^{\alpha} = 0.05$ is commonly used (Agnew and Duygulu, 2005; Wang et al., 2010), it is assumed that m^{α} are different from one deformation mechanism to another in the current study.

The use of different SRSs can either introduce numerical instability when the time step is large (e.g., $\Delta t = 0.1$ s) or leads to extremely long computational time when the time step has to be forcibly small. Generally, a smaller time step is required to stabilize the calculation through reducing the stress or strain fluctuation at a time step. In the present work, an adaptive time step is used to balance both the numerical stability and the computational time (Asaro and Needleman,

1985; Wu et al., 1996). First, the time step is limited such that maximum absolute shear strain increments over all grains and systems is less than a threshold value, i.e.

$$|\dot{\gamma}^{\alpha}_{max}|\Delta t < \Delta\gamma_T \tag{2}$$

where $\dot{\gamma}^{\alpha}_{max}$ is the maximum shear rate, and $\Delta\gamma_T$ is a threshold value for shear rate increment. Second, the maximum von Mises stress increment over all grains is less than a threshold value,

$$\Delta\sigma^{e}_{max} < \Delta\sigma_T \tag{3}$$

where $\Delta\sigma^{e}_{max}$ is the maximum von-Mises stress increment. The threshold stress increment $\Delta\sigma_T$ is calculated through $\phi\,\tau^{0}_{min}/C_e$, where τ^{0}_{min} is the minimum initial critical resolved shear stress over all slip/twinning systems (τ_0 of basal slip in current study), $C_e = \sqrt{C_{ij}C_{ij}}$ represents the magnitude of the elastic constants C_{ij}, and ϕ is a coefficient to control the stress increment. These two strategies were found be able to significantly improve numerical stability and meanwhile reduce computational cost.

The TDT scheme was developed to treat both twinning and de-twinning activities. A new twin is firstly created by Twin Nucleation (TN) within an existing twin-free grain. The orientations of the new grain and the original grain are related to via the twin relationship. In the old version of TDT scheme, a twin may not be nucleated; however, a zero-volume grain is still created via twin relationship to account for the possible twinning. Therefore, there are many "ghost grains" with zero volume fractions, which intensifies numerical instability (Wang et al. 2013b) when treating separate or small SRSs. In the present improved version, only when the twinned volume fraction reaches a critical value (here 0.1%), a twin is nucleated with an initial volume fraction of 0.1% of the original un-twinned grain volume, and the volume of the matrix is simultaneously decreased by the same amount. This treatment stabilizes the numerical calculation even when different SRSs are assigned to the deformation mechanisms. After nucleation, the twins can grow (twinning) or shrink (de-twinning) without changing the total combined volume fraction of the twins and matrix. As strain proceeds, the matrix and twins are allowed to develop as independent inclusions in the homogeneous effective medium.

Twin growth (TG) is achieved via twinning operations of twin propagation (TP) and matrix reduction (MR). Twin shrinkage (TS) is achieved via de-twinning operations of twin reduction (TR) and matrix propagation (MP). Twinning operation of MR and de-twinning operation of MP

are driven by the stress of the matrix, while de-twinning operation of TR and twinning operation of TP are driven by the stress of the twins. Furthermore, the plastic strain rate due to MR (twinning) and MP (de-twinning) is ascribed to the matrix, while the plastic strain rate due to TP (twinning) and TR (de-twinning) is ascribed to the twin. The shear rate associated with twinning system α is assumed analogous to that for slip (Eq. 3) if the RSS τ^α is in the appropriate direction:

For matrix reduction (MR) or twin reduction (TR) (denoted by *I*):

$$\dot{\gamma}_I^\alpha = \begin{cases} \dot{\gamma}_0 |\tau^\alpha / \tau_{cr}^\alpha|^{1/m^\alpha} & \tau^\alpha > 0 \\ 0 & \tau^\alpha \leq 0 \end{cases} \quad (4)$$

and for matrix propagation (MP) or twin propagation (TP):

$$\dot{\gamma}_I^\alpha = \begin{cases} -\dot{\gamma}_0 |\tau^\alpha / \tau_{cr}^\alpha|^{1/m^\alpha} & \tau^\alpha < 0 \\ 0 & \tau^\alpha \geq 0 \end{cases} \quad (5)$$

For MR and MP, the RSS τ^α, is calculated from the stress in the matrix, with τ_{cr}^α the CRSS on twin system α. For TP and TR, τ^α is calculated from the stress in the twin, with τ_{cr}^α the CRSS on twin system α. The corresponding changes in the twin volume fractions for MR, MP, TP and TR are thus given by:

$$\dot{f}_{MR}^\alpha = |\dot{\gamma}_{MR}^\alpha| / \gamma^{tw},\ \dot{f}_{MP}^\alpha = -|\dot{\gamma}_{MP}^\alpha| / \gamma^{tw},\ \dot{f}_{TP}^\alpha = |\dot{\gamma}_{TP}^\alpha| / \gamma^{tw} \text{ and } \dot{f}_{TR}^\alpha = -|\dot{\gamma}_{TR}^\alpha| / \gamma^{tw} \quad (6)$$

where the characteristic twinning shear strain γ^{tw} is chosen to be 0.129 for extension twinning in magnesium alloys (Kelly and Hosford, 1968). The net rate of change of the twin volume fraction associated with twinning system α is:

$$\dot{f}^\alpha = f^M \left(\dot{f}_{MR}^\alpha + \dot{f}_{MP}^\alpha \right) + \sum_\alpha f^\alpha \left(\dot{f}_{TR}^\alpha + \dot{f}_{TP}^\alpha \right) \quad (7)$$

where f^M is the volume fraction of the matrix calculated in terms of $f^M = 1 - f^{tw} = 1 - \sum_\alpha f^\alpha$.

A threshold for twinning is defined since a grain is rarely twinned entirely (i.e., volume fraction of the matrix is always non-zero):

$$V^{th} = \min(1.0, A_1 + A_2 V^{eff} / V^{acc}) \quad (8)$$

The threshold value V^{th} is the point where the given grain is twin-terminated. Additional twinning is not allowed once V^{th} has been reached by the combined volume fraction of all twins. V^{eff} is the volume fraction of twin-terminated grains, and V^{acc} is the total accumulated twin

volume fraction in the polycrystal. Two optimized fitting parameters (A_1 and A_2) are introduced to tailor the evolution of V^{th}.

The CRSS evolves as:

$$\dot{\tau}_{cr}^{\alpha} = \frac{d\hat{\tau}^{\alpha}}{d\Gamma} \sum_{\beta} h^{\alpha\beta} \left| \dot{\gamma}^{\beta} \right| \tag{9}$$

where Γ is the accumulated shear strain in the crystal and calculated in terms of $\Gamma = \sum_{\alpha} \int |\dot{\gamma}^{\alpha}| dt$, and $h^{\alpha\beta}$ are the latent hardening coupling coefficients. The hardening coupling coefficients are used to empirically consider the obstacles on system α associated with system β. $\hat{\tau}$ is the threshold stress defined by an extended Voce law:

$$\hat{\tau} = \tau_0 + (\tau_1^{\alpha} + h_1^{\alpha}\Gamma)\left(1 - \exp\left(-\frac{h_0^{\alpha}}{\tau_1^{\alpha}}\Gamma\right)\right) \tag{10}$$

where τ_0 and $\tau_0 + \tau_1$ are the initial and back-extrapolated CRSSs, h_0 and h_1 are the initial and the asymptotic hardening rates, respectively.

De-twinning activity mainly occurs during reverse loading upon previous twining activity. The cases studied in the current work involve merely twinning, therefore $\dot{\gamma}_{MR}^{\alpha}$, $\dot{\gamma}_{TR}^{\alpha}$, $\dot{f}_{MP}^{\alpha}$ and $\dot{f}_{TP}^{\alpha}$ are nearly zero in all the simulations. As a consequence, the macroscopic effect associated with different microscopic SRS's in current study does not depend on the addition of detwinning. In other words, the proposed methodology would be appropriate for applications to materials deforming only by deformation slips with diverse SRSs.

The Affine linearization scheme is employed in the current work since it has the best overall performance for metallic materials with HCP (Wang et al., 2010a, b, d; Qiao et al., 2015b) or face centered cubic (FCC) crystal structures (Guo et al., 2015).

3. Results and discussion

In this section, based on the experimentally obtained SRSs of magnesium alloys summarized in Introduction, the SRSs of the deformation mechanisms of AZ31 magnesium alloys at room temperature are determined by combining a stress relaxation test and the EVPSC polycrystal plasticity model. Later, the determined SRSs are validated by their application to another magnesium alloy AZ31B sheet independent from the stress relaxation test.

3.1 SRSs of deformation mechanisms

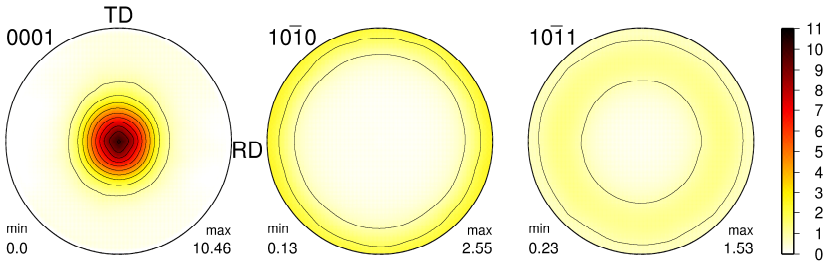

Figure 1. Initial texture of the AZ31 plate (Wang et al., 2016a).

The material studied here is an AZ31 alloy plate, with typical rolled initial texture (Fig. 1). In order to see the activities of deformation mechanisms of magnesium alloys under different loading paths, simulations of in-plane tension, in-plane compression and compression along normal direction (ND) of the plate are performed. The hardening parameters and SRS are adopted from previously published results for the AZ31 alloy sheet (Wang et al., 2010a). Fig. 2 shows the typical stress-strain response and relative activities of various deformation mechanisms calculated by the EVPSC model. The activities under in-plane tension (Fig. 2b) and compression along ND (Fig. 2f) remain nearly steady in terms of the strain level. Fig. 2c and 2d shows the S-type stress-strain curve of AZ31 plates under in-plane compression and the corresponding relative activities of deformation mechanisms. Basal slip and extension twinning play dominant roles for the strain range of 0 to 0.04, whereas prismatic slip activity increases over the strain range from 0.04 to 0.08 while twinning activity decreases. Pyramidal slip is activated and enhanced over the strain range from 0.08 to 0.12 at which point the stresses are relatively high compared to the other loading orientations. In contrast to in-plane tension and compression along the ND, in-plane compression is governed by different deformation mechanisms at different strain levels.

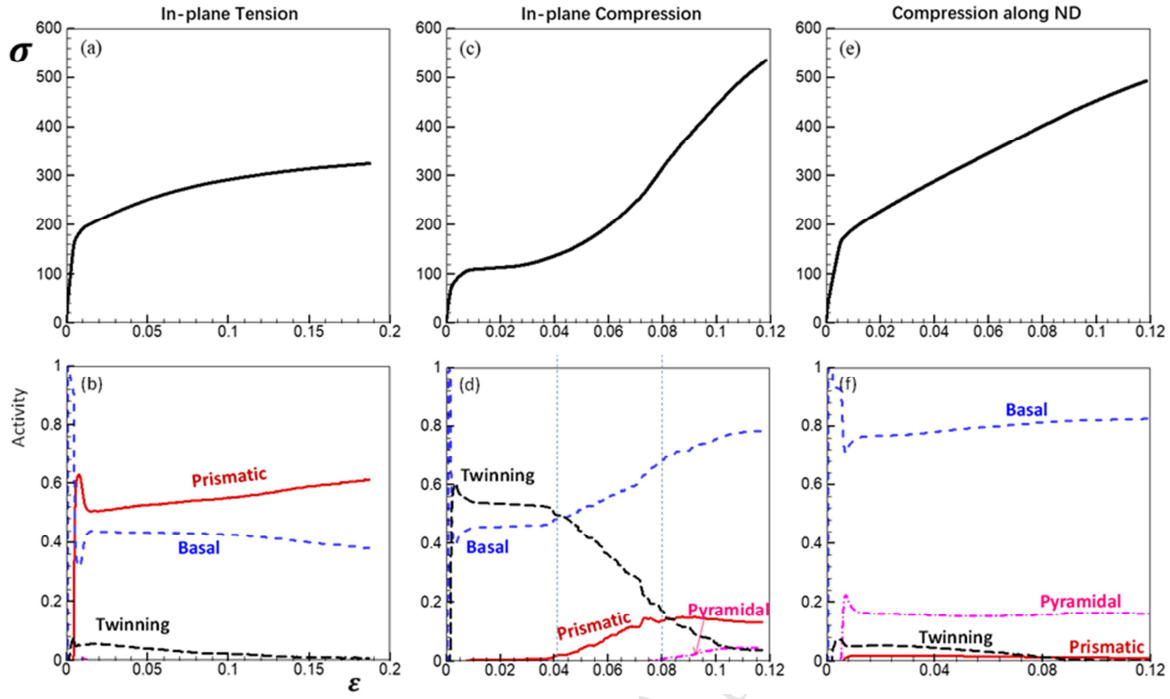

Figure 2. Typical stress-strain curves and the corresponding relative activities simulated by the EVPSC model: (a), (b) in-plane tension (c), (d) in-plane compression, and (e), (f) compression along ND.

A compressive stress relaxation test along the rolling direction (RD) of AZ31 plate was conducted by periodically holding strain constant (Wang et al., 2016a). In that work, it was demonstrated that the activities of the deformation mechanisms were not altered by the holding periods. Therefore, the variation of the active deformation mechanisms at different strain levels during in-plane compression provides an excellent opportunity to obtain both the hardening parameters and the strain rate sensitivities. These parameters associated with the EVPSC model are obtained through simultaneously fitting the stress-strain curves of uniaxial tension and compressive stress relaxation. As indicated by the relative activities of various deformation mechanisms in Fig. 2, the parameters associated with twinning and pyramidal slip were obtained through fitting compression, those associated with prismatic slip were obtained through fitting tension, and those associated with basal slip were obtained through fitting both. The fitted stress-strain curves match the measured data very well (Fig. 3). The determined hardening parameters and the strain rate sensitivities are listed in Table 1. The obtained hardening parameters are also in good consistency with those obtained by other researchers (Agnew and Duygulu, 2005; Jain

and Agnew, 2007).

The order of SRSs associated with the slip systems also reasonably agrees with the conclusions drawn by Movahedi-Rad and Alizadeh (2017), in their molecular dynamics study on dependence of strain rate sensitivity on the slip system of aluminum single crystals, that easier slip on the more compact slip planes and directions results in lower SRS values. For magnesium alloys, twinning does not follow this rule and is always nearly rate insensitive.

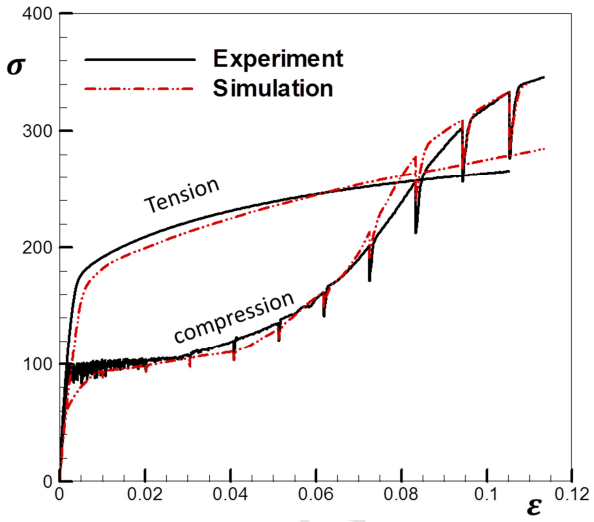

Figure 3. Experimental (Wang et al., 2016a) and simulated stress-strain curves of AZ31 plate under uniaxial tension and compression with strain holdings.

Table 1. Parameters for magnesium alloy AZ31 plate determined for the EVPSC model.

Modes	m	τ_0 (MPa)	τ_1 (MPa)	θ_0 (MPa)	h^{st} (on twin)	A_0	A_1
Basal	1/100 (0.01)	18	5	80	1	NA	NA
Prismatic	1/80 (0.0125)	105	30	300	1	NA	NA
Pyramidal	1/33 (0.03)	120	180	2000	1	NA	NA
Extension Twin	1/120 (0.0083)	30	0	0	1	0.7	0.9

Twinning is generally considered to be an athermal process, so that the stress required for twinning is expected to be largely independent of temperature and strain rate. (Korla and Chokshi, 2010). Very recently, Bhattacharyya et al. (2016) also observed that the strain-rate sensitivity of the yield strength varies with loading direction. Their experimental results further support the fact that different deformation mechanisms control yielding along the different directions, and these different mechanisms have different rate-controlling processes. For example, {10.2} extension twinning is known to be relatively rate insensitive, so the yield strength is

observed to be rate insensitive when that mechanism is dominant. Dislocation motion shows appreciable strain rate sensitivity due to its thermally activated nature (Kocks, 1975). The order of SRSs associated with deformation mechanisms can be compared to the experimental results by Karimi et al. (2013). At the temperature of 200°C, the SRS of AZ31 magnesium alloy is 0 in the twin-dominated region (strain of 0.05) and 0.03 in the twinning and basal slip region (strain of 0.2). At temperature of 300°C, the SRS is 0.08 (with error of 0.01), where prismatic cross slip is the dominant mechanism. At temperature of 400°C, the SRS is 0.14 (with error of 0.01), where pyramidal cross slip is the dominant mechanism. The strain rate can be theoretically discussed through the following equation (Kocks, et al., 1975; Kocks, 2001; Wang et al., 2017):

$$\dot{\varepsilon} = \dot{\varepsilon}_0 \exp\left(-\frac{Q_0}{kT}\left(1-\frac{\sigma}{\sigma_c}\right)^p\right)^q \tag{10}$$

where $\dot{\varepsilon}_0$, Q_0, k, T, σ, and σ_c are reference strain rate, activation energy, Boltzmann's constant, temperature, applied stress and threshold stress, respectively. p and q are parameters bounded within [0, 1] and [1,2]. Without losing generality, $p = q = 1$ are assumed here. The SRS (m value) can be derived as:

$$m = \frac{\partial ln\sigma}{\partial ln\dot{\varepsilon}} = \frac{\sigma_c}{\sigma}\frac{kT}{Q_0} \tag{11}$$

In plastic regime, where σ_c/σ can be estimated to be 1, the SRS is strongly dependent on temperature. Accordingly, the room temperature SRS (m^{RT}) can be estimated by

$$m^{RT} = \frac{T_{RT}}{T} m(T) \tag{12}$$

As a consequence, the SRSs for basal slip, prismatic slip, pyramidal slip at room temperature (298°K) are 0.018, 0.04 and 0.06, respectively. The order of these SRSs is in good agreement with the estimated SRSs in current work, though there is discrepancy between their absolute values. This discrepancy is possibly due to the occurrence of dynamic recrystallization at elevated temperatures (Karimi et al., 2013).

3.2 Effect of SRSs on stress relaxation test

In order to assess the potential benefit of employing the SRS individually for each deformation mechanism, the stress-strain response using a uniform SRSs for all of the mechanisms (as has been used in the simulation practices to-date) is also calculated for contrast.

Four different uniform SRSs ranging from 0.0083 to 0.03, together with the hardening parameters listed in Table 1, were tried. Fig. 4 shows the comparison between the experimental and simulated results. Compared to the experimental results, adoption of larger SRS values provides reasonable stress drops at higher strain levels (Fig. 4a and 4b), while using smaller SRS values gives good results at lower strain levels (Fig. 4c and 4d). However, none of the applied single SRSs can predict stress drops consistent with the experimental data over the entire strain range. Fig. 5 presents the comparison between the predicted stress drops and the experimental values in terms of the holding strain. Consistent with Fig. 3 and Fig. 4, only the stress drops predicted using different SRSs for each deformation mechanism agree well with the experimental data throughout the entire strain range; using a single SRS leads to obvious deviation in a certain range of strain. Therefore, it should be better to use separate SRSs for each deformation mechanism to predict and interpret the rate dependent behaviors of the alloy.

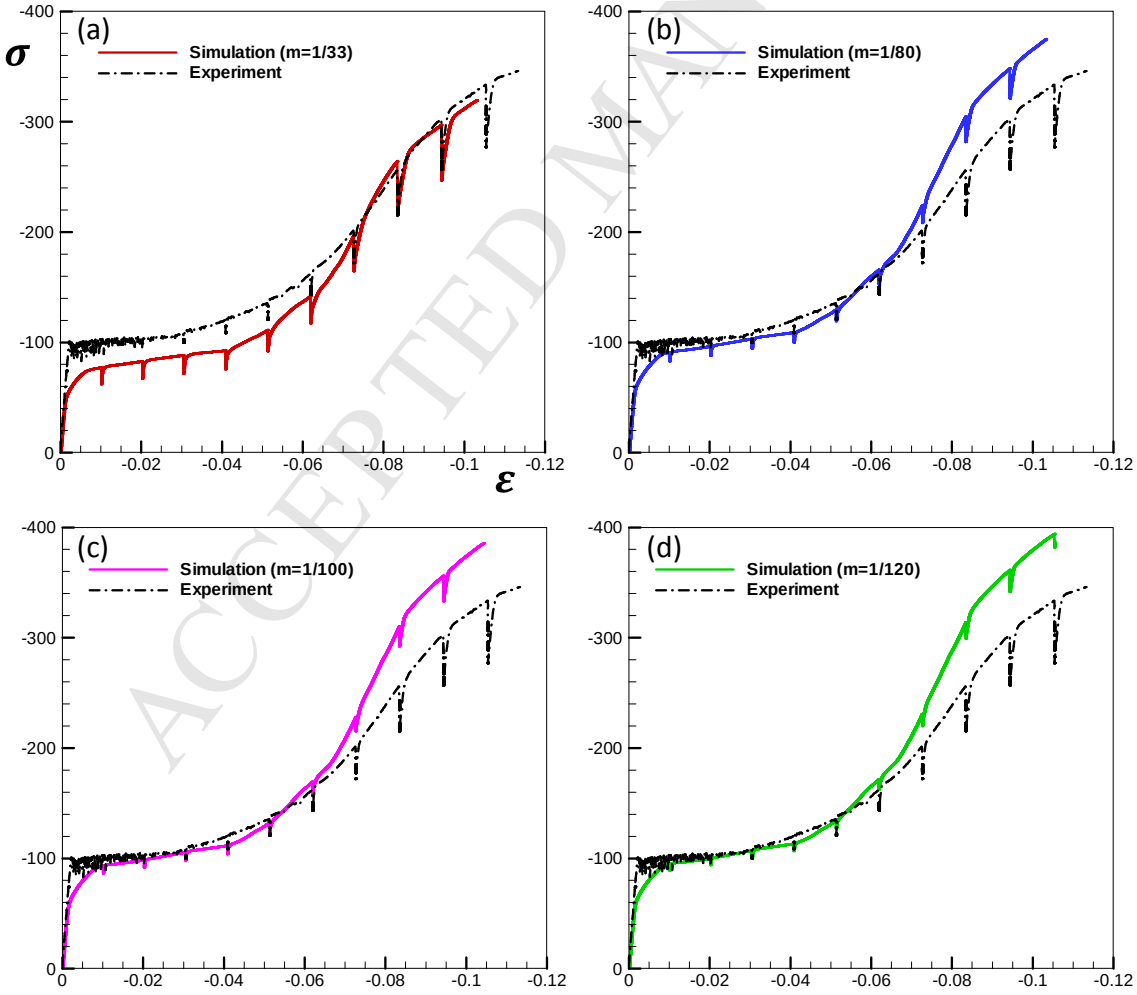

Figure 4. The simulated and measured (Wang et al., 2016a) stress-strain response of AZ31 plate under compression with strain holdings by using single rate sensitivity for all the four deformation mechanisms.

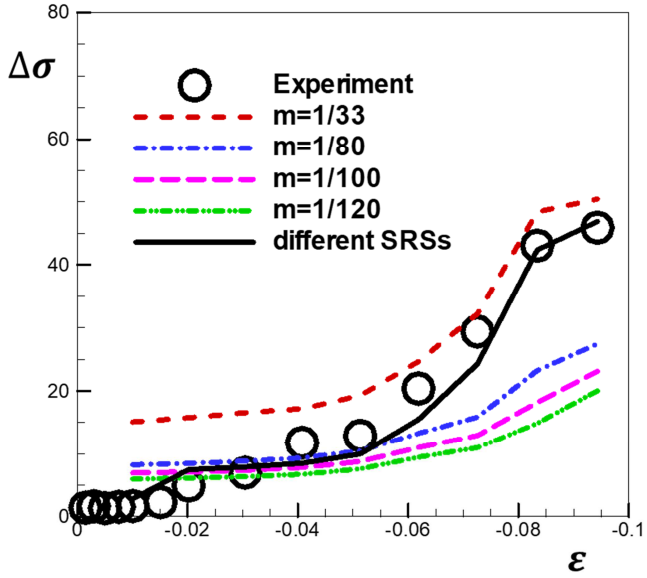

Figure 5. Experimental (Wang et al., 2016a) and predicted stress drop versus holding strain.

3.3 Effect of SRSs on internal elastic strain

The evolution of internal elastic strains under in-plane compression has been measured through in-situ neutron diffraction measurement using the Spectrometer for Materials Research at Temperature and Stress (SMARTS) at LANSCE. Detailed description of the experimental procedure can be found elsewhere (Wang et al., 2016a). The internal elastic strain is the relative change in average lattice spacing d, i.e. $\varepsilon^{hk.l} = (d^{hk.l} - d_0^{hk.l})/d_0^{hk.l}$, where d_0 is the stress-free reference lattice spacing. This strain is purely elastic and induced by the stress in the subset of grains (*hk.l*). The internal elastic strain increases linearly with the macroscopic stress in the elastic regime. The increasing slope is a function of the bulk crystallographic texture and the directional Young modulus $E_{hk.l}$.–Typically, the subsets of grains in 'soft' orientations tend to yield first and stop bearing any internal elastic stress, while those in 'hard' orientations continue elastic deformation. Because the macroscopic stress is the self-consistently average stress of all the grains, plastic relaxation in one subset of grains can increase stress loading in others. The internal elastic strain deviation from linearity imply that plastic strain is occurring within grains in some subsets. As a consequence, the inflections in the curves are related to activities of specific slip and twinning systems.

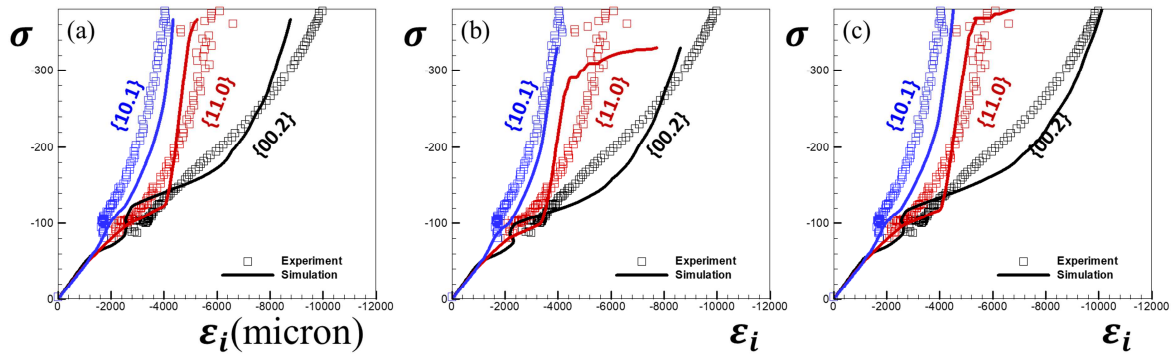

Figure 6. Internal elastic strain evolution of AZ31 plate under in-plane compression using: (a) different SRSs for different mechanism; (b) $m = 0.03$ for all mechanisms; and (c) $m = 0.0125$ for all mechanisms.

Fig. 6a shows the comparison between the measured and predicted internal elastic strains (ε_i) of {00.2}, {11.0} and {10.1} diffraction planes under monotonic compression, where all the deformation mechanisms of interest play distinct roles. The yield stress is about 100 MPa, which coincides with the plateau in the compressive stress - strain curve where the twinning activity dominates (see Figs. 3). An obvious stress transfer occurs while twinning reorients the {00.2} diffraction planes 'into' the detector. This ''shear over-relaxation'' effect associated with twinning usually leads to abrupt lattice strain evolution as predicted by the model, while this phenomenon is weakened during diffraction measurement (Clausen et al., 2008; Aydiner et al., 2009). Therefore, the measured lattice strain at the yielding point cannot be accurately captured by the model.

Twinning is responsible for the dispersion observed for {11.0} peaks above 300 MPa, because twinning reorients the grains that contribute to the peak and only a small volume fraction remains. For comparison purpose, the internal elastic strains predicted by $m = 0.03$ and $m = 0.0125$ are also presented and compared with the experimental values, as shown in Fig. 6b and 6c. All the three predictions can capture the evolution tendency of the internal elastic strain measured by neutron diffraction. Among them, the predicted results using separate SRSs and a single value of $m = 0.0125$ are better than those predicted using a single value of $m = 0.03$. If one observes carefully, the simulation of using separate SRSs is slightly better than that by using $m = 0.0125$, especially for the {11.0} diffraction plane, where the much shifted internal strain

after the stress exceeds 360MPa is not observed from experiment. The plastic deformation of grains with the three diffraction planes ({00.2}, {11.0} and {10.1}) are dominated by pyramidal slip, prismatic slip and basal slip, respectively. At a given shear rate, the value of SRS governs the resolved shear stress (RSS) of a slip/twinning system. The RSSs on all the active systems determine the stress state and therefore the elastic deformation of each grain. Using multiple SRSs leads to more realistic elastic deformation of grains, and thus better internal elastic prediction.

The predicted textures at strains of 5% and 10% under in-plane compression using separate SRSs are depicted in Fig. 7. The results are consistent with both experimental and previous simulated results (Agnew and Duygulu, 2005; Wang et al., 2010a). Through comparing to others obtained by using a single value of SRS (0.03 and 0.0125, respectively), the effect of SRSs on the texture evolution is found to be minor.

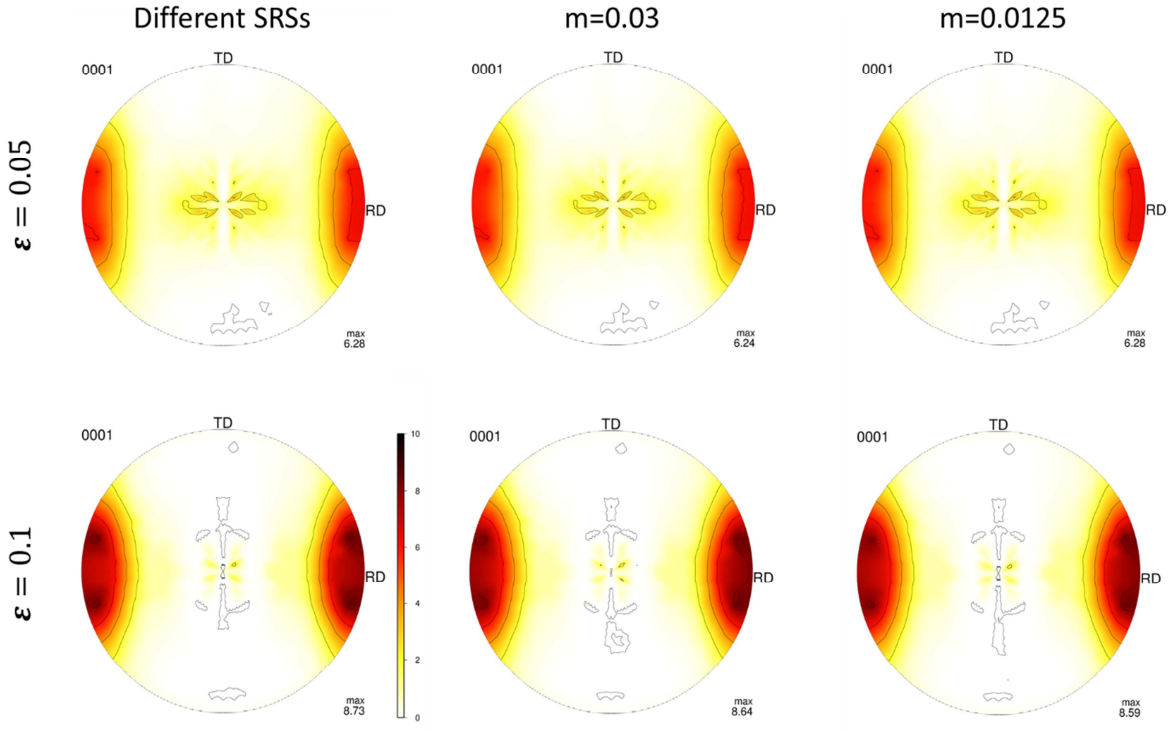

Figure 7. Predicted textures at strains of 5% and 10% under in-plane compression using: (a) different SRSs for different mechanism; (b) $m = 0.03$ for all mechanisms; and (c) $m = 0.0125$ for all mechanisms.

3.5 Application to other loading cases

This section considers the application of the determined SRSs to a similar magnesium alloy but alternate loading and strain rate cases. We apply these SRSs to simulate the experiments carried out by Kurukuri et al. (2014a) on the strain rate sensitivity and tension-compression asymmetry of an AZ31B alloy sheet with the initial rolling texture as in Fig. 8. In that study, room temperature tensile and compressive tests were carried out at strain rates ranging from 10^{-3} to 10^{3}/s. The high strain rate cases ($\dot{\varepsilon} > 10s^{-1}$), involve intensive dynamic response and are not investigated in current study. The experimental results shown in Fig. 9 (Kurukuri et al., 2014a) clearly show the strain rate sensitivity and its effects on the behaviors in the deformation of in-plane tension, in-plane compression and compression along ND. The effects of strain rate on the three types of tests in Fig. 9 are different from each other. The strain rate effect on the stress-strain response of compression along the ND is relatively larger than that of in-plane tension (see Fig. 9d). The strain rate effects on these two tests are steady throughout the entire straining. In contrast, strain rate effect in RD compression is neglectable until strain reaches about 0.04, and thereafter becomes remarkable. In addition to the SRSs, the other modeling parameters for the rolled sheet, which are different from the AZ31 plate mentioned in Section 3.1 due to different processing history, are determined by simultaneously fitting both the uniaxial tension and compression tests (as shown in Fig. 10). Table 2 lists the determined hardening parameters, along with the rate sensitivities obtained in Section 3.1, which will be used for all the following simulations.

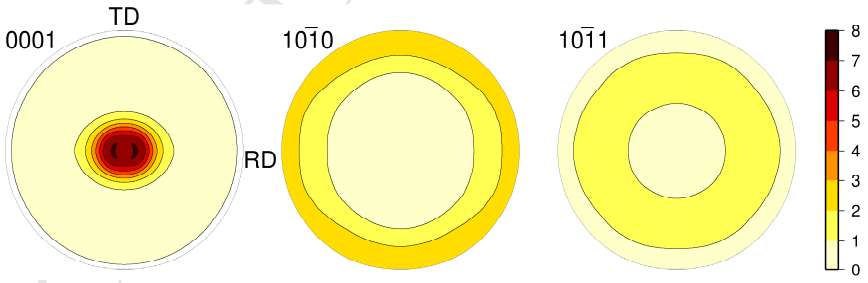

Figure 8. Initial texture of the AZ31B sheet, reproduced from Kurukuri et al. (2014a).

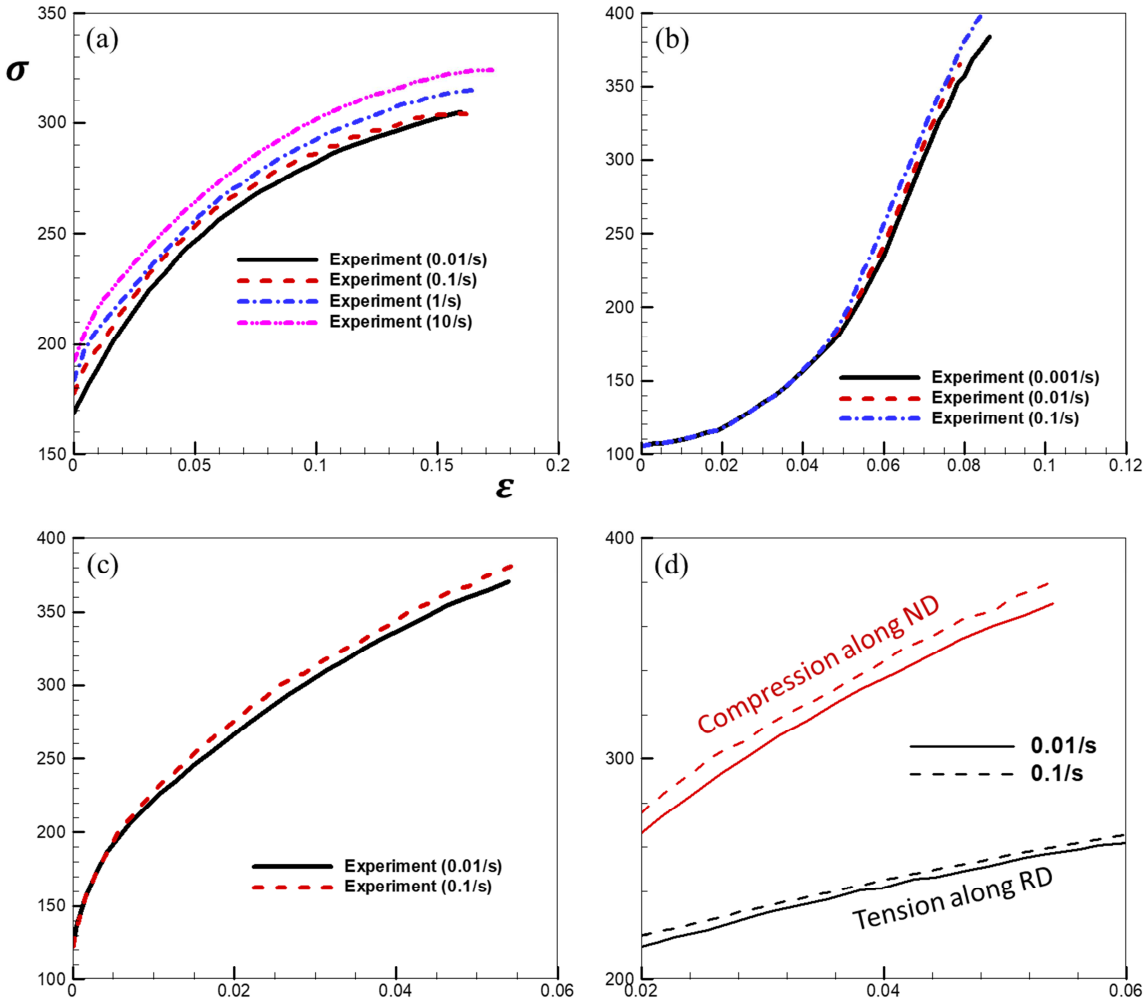

Figure 9. Experimental (Kurukuri et al., 2014a) stress-strain curves at different loading rates for (a) tension along RD, (b) compression along RD, (c) compression along ND, and (d) magnified comparison between (a) and (c).

Table 2. Parameters of magnesium alloy AZ31B determined for the EVPSC model.

Modes	m	τ_0 (MPa)	τ_1 (MPa)	θ_0 (MPa)	h^{st} (on twin)	A_0	A_1
Basal	0.01	15	5	80	1	NA	NA
Prismatic	0.0125	87	60	400	1	NA	NA
Pyramidal	0.03	130	280	1400	2.8	NA	NA
Extension Twin	0.0083	41	0	0	1	0.41	1

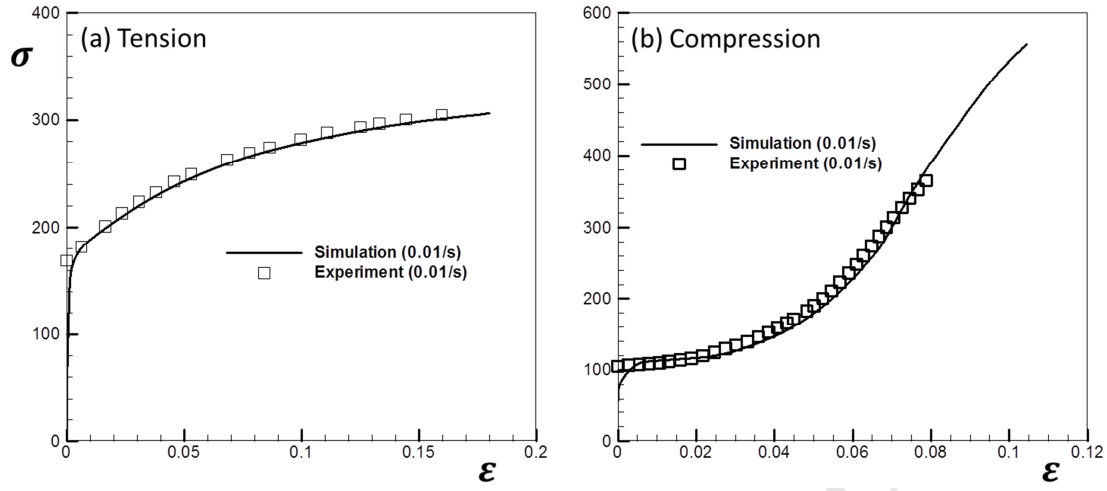

Figure 10. Experimental (Kurukuri et al., 2014a) and simulated stress-strain response of magnesium alloy AZ31B under uniaxial tension and compression along RD.

Figs. 11 and 12 show the measured and predicted results for the AZ31B alloy sheet under in-plane tension along the RD and Transverse Direction (TD) and at strain rates of 0.01, 0.1, 1.0 and10 s^{-1}, respectively. The EVPSC model using separate SRSs accurately reproduce the stress-strain response for in-plane tension. As shown in Fig. 2b, the main active deformation mechanisms under in-plane tension of AZ3B sheet are prismatic slip and basal slip. Recall that stress-strain response for in-plane tension increases with strain rate, as in Fig. 9. The increase in stress is mainly governed by the SRSs of prismatic and basal slips.

Figs. 13 and 14 show the results for the AZ31B sheet under in-plane compression (along both RD and TD) at strain rates of 0.001, 0.01 and 0.1 s^{-1}. The simulated stress-strain responses of in-plane compression is also in good consistency with the experimental ones. The variation of rate dependency under in-plane compression, as shown in Fig.8b, is greatly related to the transition of active deformation mechanisms shown in Fig. 2d. During in-plane compression, the nearly strain rate insensitivity the AZ31B sheet before 0.04 strain is correspondent to the dominancy of twinning mechanism shown in Fig.2d, and the increase of strain rate effect at higher strains results from the more activities of slips. The EVPSC model employing separate SRSs can successfully capture the complicated strain rate response during the in-plane compression of the AZ31B sheet. As can be seen, a better match between experiments and predictions is obtained under both tension and compression along RD (Figs. 11 and 13) than that

along TD (Figs. 12 and 14). Specifically, the hardening rate under tension along TD is predicted to be higher than the experimental data (Fig. 12). The AZ31B sheet exhibits in-plane anisotropic behavior as more grains orientate with the c-axis spreading wider along the RD (Fig. 8), while the hardening parameters are determined from the mechanical behaviors along RD. However, the rate dependent behaviors concerned in current study are successfully captured by using the proposed methodology of using multiple SRSs.

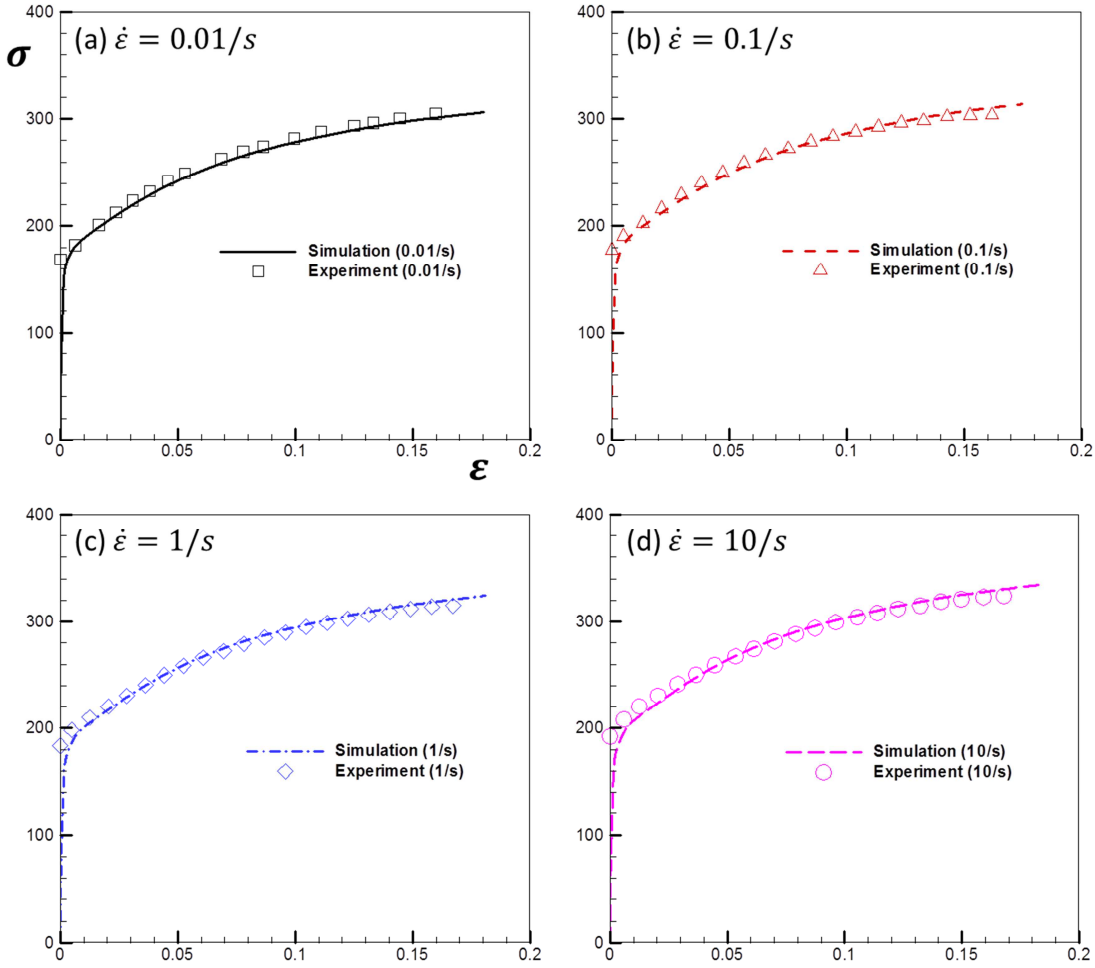

Figure 11. Experimental (Kurukuri et al., 2014a) and predicted stress-strain curves of magnesium alloy AZ31B sheet under uniaxial tension with different strain rates along RD.

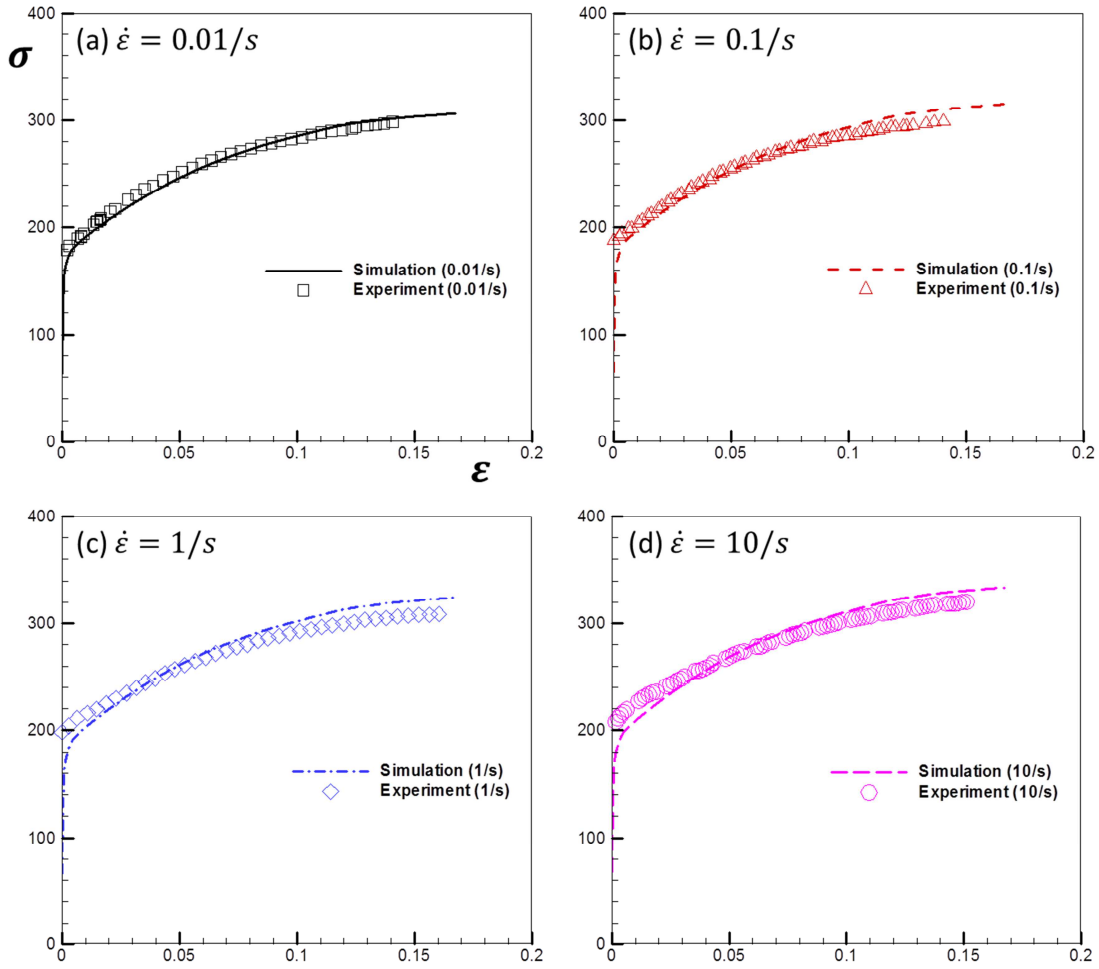

Figure 12. Experimental (Kurukuri et al., 2014a) and predicted stress-strain curves of magnesium alloy AZ31B sheet under uniaxial tension with different strain rates along TD.

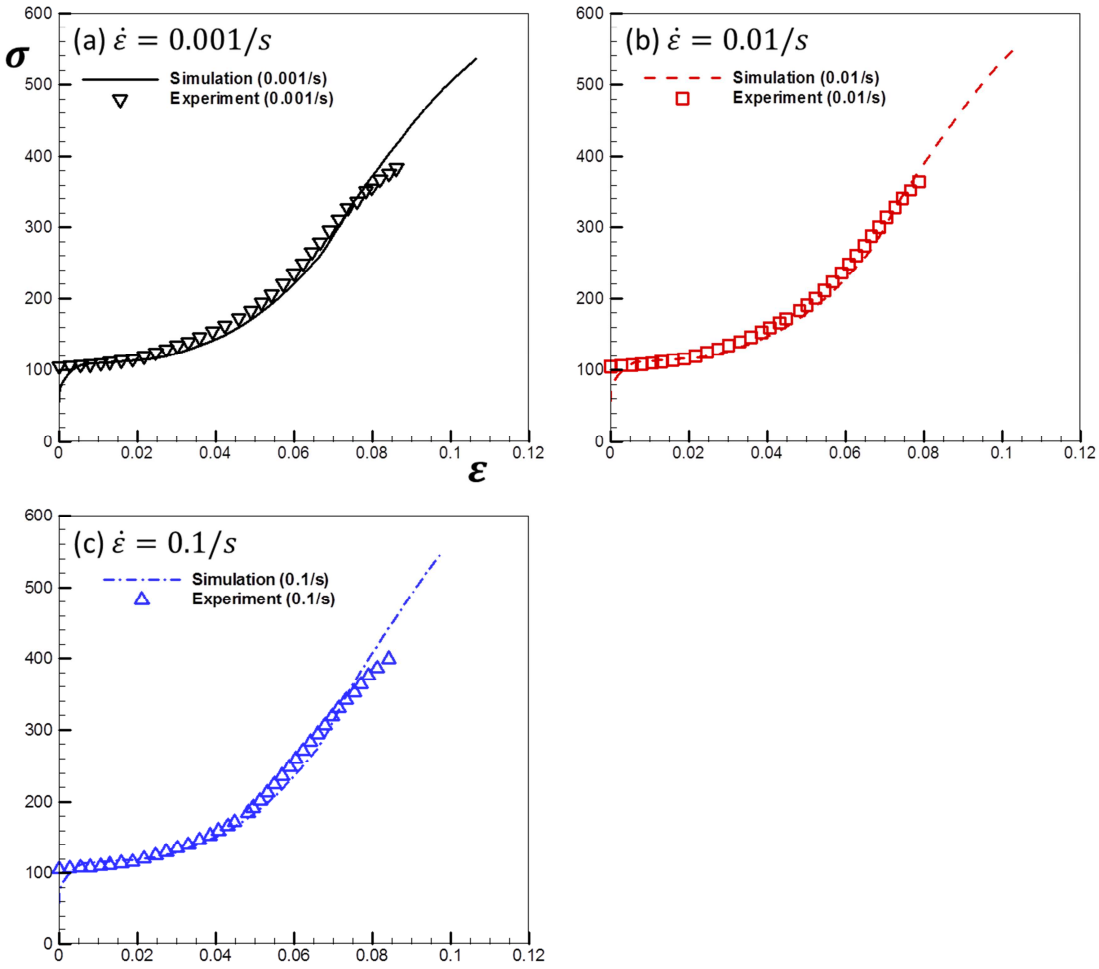

Figure 13. Experimental (Kurukuri et al., 2014a) and predicted stress-strain curves of magnesium alloy AZ31B sheet under uniaxial compression with different strain rates along RD.

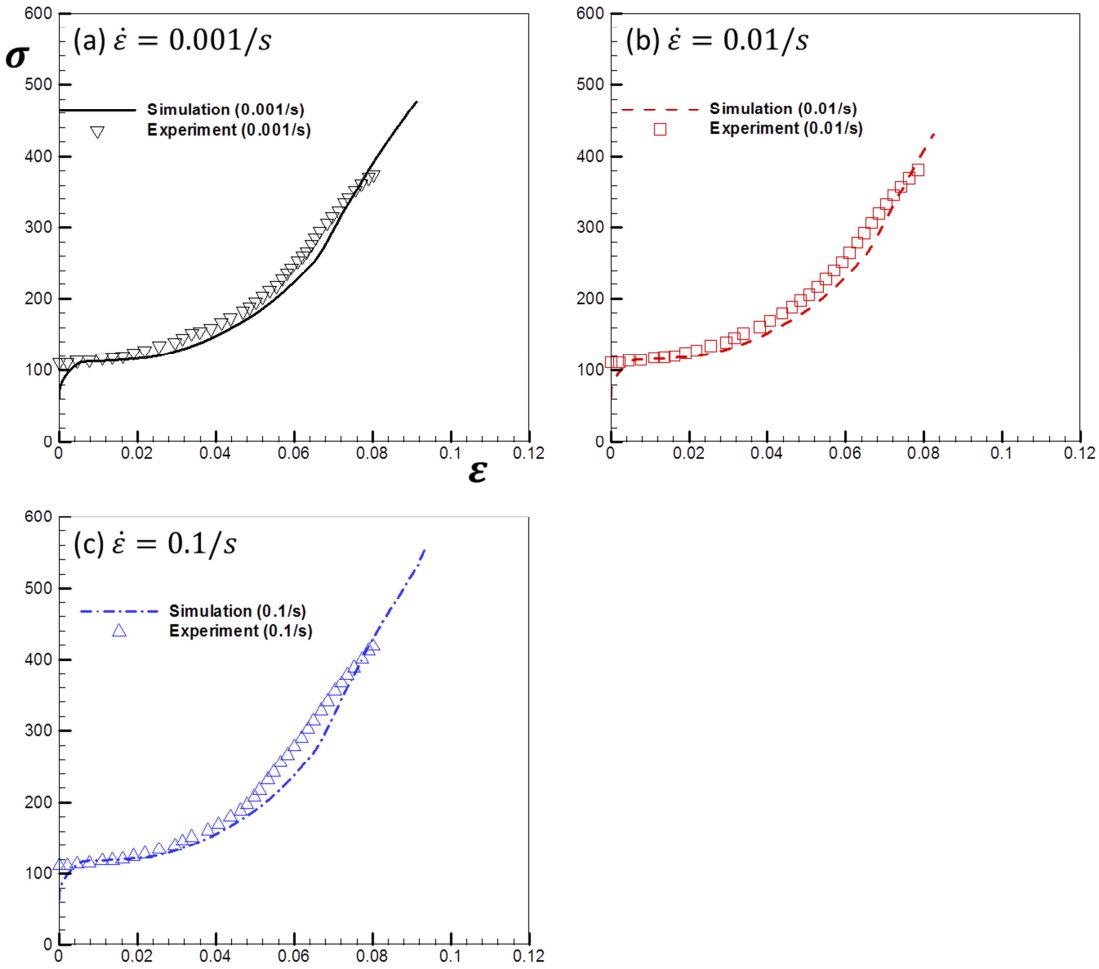

Figure 14. Experimental (Kurukuri et al., 2014a) and predicted stress-strain curves of magnesium alloy AZ31B sheet under uniaxial compression with different strain rates along TD.

Fig. 15 shows the good agreement between experimental and predicted results of the AZ31B sheet under compression along ND at strain rates of 0.01 and 0.1 s^{-1}. Corresponding to the main active deformation mechanisms with obvious strain rate sensitivity, basal slip and pyramidal slip, as shown in Fig.2f, the stress-strain response of ND compression increases with increasing strain rate as in Fig. 9. From Fig. 15, it can be concluded that the determined SRSs for basal slip and pyramidal slip can correctly predict the strain rate effect on the stress-strain response.

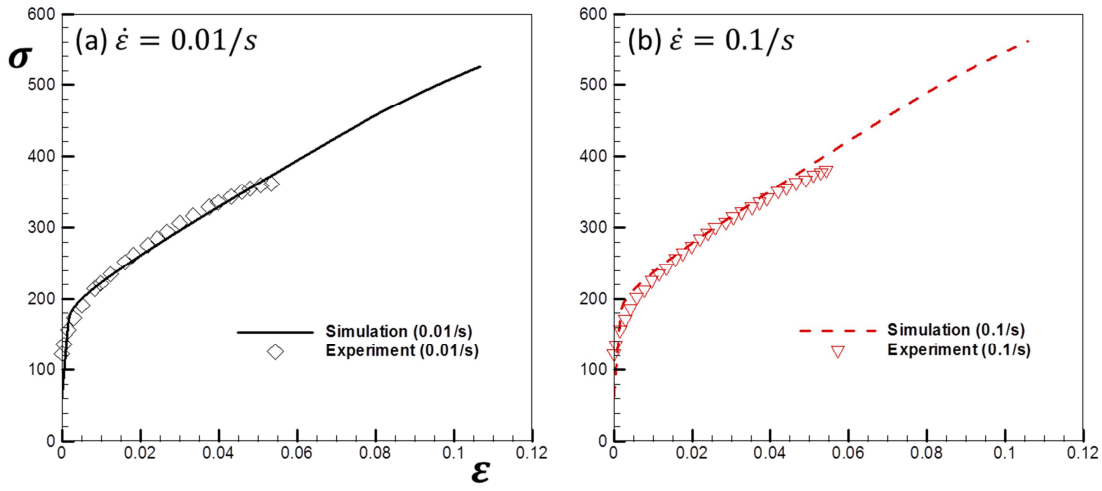

Figure 15. Experimental (Kurukuri et al., 2014a) and predicted stress-strain curves of magnesium alloy AZ31B sheet under uniaxial compression along ND at different strain rates.

Figs. 3, 6, 11 to 15 have demonstrated the excellent capability of the EVPSC model, employing separate SRSs for different deformation mechanisms, in describing the strain rate effect of magnesium alloys. In current work, the SRSs of the deformation mechanisms, basal slip, prismatic slip, pyramidal slip and extension twinning are 0.01, 0.0125, 0.03, and 0.00825, respectively. The strain rate related experimental results can be reasonably reproduced by employing these values, and the rate dependent behaviors of magnesium alloys can be well interpreted by the sensitivity of deformation mechanisms. Given that the magnesium alloys in the current study show a positive rate-dependent effect, all the SRSs are greater than zero. It should be pointed out that the SRSs for basal slip and extension twinning are small enough to represent their nearly rate-insensitive characteristic. According to our calculations, using even smaller SRSs will not change the simulation results significantly.

4. Conclusions

Experimental observations on rate-dependent behaviors of magnesium and its alloys suggest different SRSs for the different operative deformation mechanisms. Taking advantage of the viscous nature of the EVPSC model, the SRSs for different deformation mechanisms were determined through combining the tests of compressive stress relaxation and uniaxial tension.

The determined SRSs were then used to study the internal elastic strain and strain rate-sensitive behavior of magnesium alloys. The following conclusions can be drawn:

1) An adaptive step method, though simple, is effective to enhance the numerical stability of the EVPSC model when treating multiple and small SRSs for magnesium alloys with multiple systems. The rate sensitivity of magnesium and its alloys can be better described by using multiple SRSs associated to operative deformation mechanisms.
2) The SRSs for different deformation mechanisms of AZ31 alloy sheet can be determined from stress relaxation tests. The values are 0.0125, 0.01, 0.03 and 0.00825 for prismatic slip, basal slip, pyramidal slip and extension twinning, respectively. The order of SRSs associated to different deformation mechanisms of AZ31 alloy is similar to that of aluminum, i.e. easier slip on the more compact slip planes and directions results in lower SRS values, except for twinning that is always nearly rate insensitive.
3) The application of the determined SRSs can reasonably capture the evolution the internal elastic strain under loading, which has been challenging for polycrystal plasticity modeling.
4) The independently studied strain rate sensitivity experiments on another AZ31 sheet have been modelled using the EVPSC model. Good agreement between the experiment and prediction results proves good adaptability of the determined SRSs to other similar magnesium alloys.

Acknowledgement

HW, PDW, SK and MW were supported by the Natural Sciences and Engineering Research Council of Canada (NSERC) and the Ontario Ministry of Research and Innovation (OMRI). SK and MW were also supported by Automotive Partnerships Canada and the Canada Research Chairs Secretariat. DL acknowledges the support of the National Natural Science Foundation of China (No. 51675331). DT gratefully acknowledges the funding for this research from the National Natural Science Foundation of China (Project No. 51575346). HW and DL thank the support of Materials Genome Initiative Center, Shanghai Jiao Tong University.

References

Abdolvand H., Daymond M.R., Mareau C., 2011. Incorporation of twinning into a crystal plasticity finite element model: evolution of lattice strains and texture in Zircaloy-2. International Journal of Plasticity 27, 1721-1738.

Agnew S.R., Duygulu O., 2005. Plastic anisotropy and the role of non-basal slip in magnesium alloy AZ31B. International Journal of Plasticity 21, 1161-1193.

Ang H.Q., Zhu S., Abbott T.B., Qiu D., Easton M.A., 2017. Strain-rate sensitivity of die-cast magnesium-aluminium based alloys. Materials Science and Engineering A699, 239-246.

Asaro R.J., Needleman A., 1985. Texture development and strain hardening in rate dependent polycrystals. Acta Metallurgica et Materialia 33, 923-953.

Aydiner C.C., Bernier J.V., Clausen B., Lienert U., Tome C.N., Brown D.W., 2009. Evolution of stress in individual grains and twins in a magnesium alloy aggregate. Physical Review B 80, 024113.

Beer A.G., Barnett M.R., 2006. Influence of initial microstructure on the hot working flow stress of Mg-3Al-1Zn. Materials Science and Engineering A423, 292-299.

Beyerlein I.J., Tomé C.N., 2008. A dislocation-based constitutive law for pure Zr including temperature effects. International Journal of Plasticity 24, 867-895.

Bhattacharya B., Niewczas M., 2011. Work-hardening behaviour of Mg single crystals oriented for basal slip. Philosophical Magazine 91, 2227-2247.

Bhattacharyya J.J., Wang F., Wu P.D., Whittington W., El Kadiri H., Agnew S.R., 2016. Demonstration of alloying, thermal activation, and latent hardening effects on quasi-static and dynamic polycrystal plasticity of a Mg alloy, WE43-T5, plate. International Journal of Plasticity 81, 123-151.

Bronkhorst C.A., Hansen B.L., Cerreta E.K., Bingert J.F., 2007. Modeling the microstructural evolution of metallic polycrystalline materials under localization conditions. Journal of the Mechanics and Physics of Solids 55, 2351-2383.

Chun Y.B., Davies C.H.J., 2011. Twinning-induced negative strain rate sensitivity in wrought Mg alloy AZ31. Materials Science and Engineering A528, 5713-5722.

Clausen B., Tomé C.N., Brown D.W., Agnew S.R., 2008. Reorientation and stress relaxation due to twinning: modeling and experimental characterization for Mg. Acta Materialia 56, 2456-2468.

Dawson P.R., Boyce D.E., MacEwen S.R., Rogge R.B., 2000. Residual strains in HY100 polycrystals: comparisons of experiments and simulations. Metallurgical and Materials Transactions A31, 1543-1555.

Dawson, P.R., Boyce, D.E., MacEwen, S.R., Rogge, R.B., 2001. On the influence of crystal elastic moduli on computed lattice strains in AA-5182 following plastic straining. Materials Science and Engineering A313, 123-144.

Follansbee P., Kocks U.C., 1988. A constitutive description of the deformation of copper based on the use of the mechanical threshold stress as an internal state variable. Acta Metallurgical Et Materialia 36, 81-93.

García-Grajales J.A., Fernández A., Leary D., Jérusalem A., 2016. A new strain rate dependent continuum framework for Mg alloys. Computational Materials Science 115, 41-50.

Guo X.Q., Wu W., Wu P.D., Qiao H., An K., Liaw P.K., 2013. On the Swift effect and twinning in a rolled magnesium alloy under free-end torsion. Scripta Materialia 69, 319-322.

Guo X.Q., Wang H., Wu P.D., Mao X.B., 2015. Analysis of reversed torsion of FCC metals using polycrystal plasticity models. International Journal of Applied Mechanics 7, 1550033.

Habib S.A., Khan A.S., Gnaupel-Herold T., Lloyd J.T., Schoenfel S.E., 2017. Anisotropy, tension-compression asymmetry and texture evolution of a rare-earth-containing magnesium alloy sheet, ZEK100, at different strain rates and temperatures: Experiments and modeling. International Journal of Plasticity 95, 163-190.

Jain A., Agnew S.R., 2007. Modeling the temperature dependent effect of twinning on the behavior of magnesium alloy AZ31B sheet. Materials Science and Engineering A462, 29–36.

Karimi E., Zarei-Hanzaki A., Pishbin M.H., Abedi H.R., Changizian P., 2013. Instantaneous strain rate sensitivity of wrought AZ31 magnesium alloy. Materials and Design 49, 173-180.

Kelley E.W., Hosford W.F., (1968). The deformation characteristics of textured magnesium. Transactions of the Metallurgical Society of AIME 242, 654-661.

Khan A.S., Pandey A., Gnäupel-Herold T., Mishra R.K., 2011. Mechanical response and texture evolution of AZ31 alloy at large strains for different strain rates and temperatures. International Journal of Plasticity 27, 688-706.

Knezevic M., Zecevic M., Beyerlein I.J., Lebensohn R.A., 2016. A numerical procedure enabling accurate descriptions of strain rate-sensitive flow of polycrystals within crystal visco-plasticity theory. Computer Methods in Applied Mechanics and Engineering 308, 468-482.

Kocks U., Argon A, Ashby M., 1975. Thermodynamics and kinetics of slip. Oxford: Pergamon Press.

Kocks U., 2001. Realistic constitutive relations for metal plasticity. Materials Science and Engineering A317, 181-187.

Korla R., Chokshi A.H., 2010. Strain-rate sensitivity and microstructural evolution in a Mg-Al-Zn alloy. Scripta Materialia 63, 913-916.

Kurukuri S., Worswick M.J., Ghaffari Tari D., Mishra R.K., Carter J.T., 2014a. Rate sensitivity and tension–compression asymmetry in AZ31B magnesium alloy sheet. Philosophical Transactions. Series A, Mathematical, Physical, and Engineering Sciences 372, 20130216.

Kurukuri S., Worswick M.J., Bardelcik A., Mishra R.K., Carter J.T., 2014b. Constitutive behavior of commercial grade ZEK100 magnesium alloy sheet over a wide range of strain rates, Metallurgical and materials transactions 45A, 3321-3337

Lebensohn R.A., Kanjarla A.K., Eisenlohr P., 2012. An elasto-viscoplastic formulation based on fast Fourier transforms for the prediction of micromechanical fields in polycrystalline materials. International Journal of Plasticity 32-33, 59-69.

Lebenshon R.A., Tomé C.N., 1993. A self-consistent anisotropic approach for the simulation of plastic-deformation and texture development of polycrystals - application to zirconium alloys. Acta Metallurgica et Materialia 41, 2611-2624.

Li L., Muránsky O., Flores-Johnson E.A., Kabra S., Shen L., Proust G., 2017. Effects of strain rate on the microstructure evolution and mechanical response of magnesium alloy AZ31. Materials Science & Engineering A684, 37-46.

Molinari A., Ahzi S., Kouddane R., 1997. On the self-consistent modeling of elastic-plastic behavior of polycrystals. Mechanics of Materials 26, 43-62.

Movahedi-Rad A., Alizadeh R., 2017. Dependence of Strain Rate Sensitivity on the Slip System: A Molecular Dynamics Simulation Journal of Materials Engineering and Performance 26, 5173 – 5179.

Proust G., Tomé C.N., Jain A., Agnew S.R., 2009. Modeling the effect of twinning and detwinning during strain-path changes of magnesium alloy AZ31. International Journal of Plasticity 25, 861-880.

Qiao H., Agnew S.R., Wu P.D., 2015a. Modeling twinning and detwinning behavior of Mg alloy ZK60A during monotonic and cyclic loading. International Journal of Plasticity 65, 61-84.

Qiao H., Wu P.D., Wang H., Gharghouri M.A., Daymond M.R., 2015b. Evaluation of elastic–viscoplastic self-consistent polycrystal plasticity models for zirconium alloys. International Journal of Solids and Structures 71, 308-322.

Song W.Q., Beggs P., Easton M., 2009. Compressive strain-rate sensitivity of magnesium – aluminum die casting alloys. Materials and Design 30, 642-648.

Tang W., Halm K.L., Trinkle D.R., Koker M.K.A., Lienert U., Kenesei P., Beaudoin A.J., 2015. A study of stress relaxation in AZ31 using high-energy X-ray diffraction. Acta Materialia 101, 71-79.

Talyan V., Wagoner R.H., Lee J.K., 1998. Formability of stainless steel. Metallurgical and Materials Transactions 29A, 2161-2172.

Turner P.A., Tomé C.N., 1994. A study of residual stresses in Zircaloy-2 with rod texture. Acta Metallurgical Et Materialia 42, 4143-4153.

Ulacia I., Dudamell N.V., Galvez F., Yi S., Perez-Prado M.T., Hurtado I., 2010. Mechanical behavior and microstructural evolution of a Mg AZ31 sheet at dynamic strain rates. Acta Materialia 58, 2988-2998.

Wang H., Raeisinia B., Wu P.D., Agnew S.R., Tomé C.N., 2010a. Evaluation of self-consistent polycrystal plasticity models for magnesium alloyAZ31B sheet. International Journal of Solids and Structures 47, 2905-2917.

Wang H., Wu P.D., Neale K.W., 2010b. On the role of the constitutive model and basal texture on the mechanical behaviour of magnesium alloy AZ31B sheet. Journal of Zhejiang University SCIENCE A11, 744-755.

Wang H., Wu P.D., Tomé C.N., Huang Y., 2010c. A finite strain elastic-viscoplastic self-consistent model for polycrystalline materials. Journal of the Mechanics and Physics of Solids 58, 594-612.

Wang H., Wu Y., Wu P.D., Neale K.W., 2010d. Numerical analysis of large strain simple shear and fixed-end torsion of HCP polycrystals. Computers Materials and Continua 19, 255-284.

Wang H., Wu P.D., Tomé C.N., Wang J., 2012a. Study of lattice strains in magnesium alloy AZ31 based on a large strain elastic-viscoplastic self-consistent polycrystal model. International Journal of Solids and Structures 49, 2155-2167.

Wang H., Wu P.D., Tomé C.N., Wang, J., 2012b. A constitutive model of twinning and detwinning for hexagonal close packed polycrystals. Materials Science and Engineering A555, 93-98.

Wang H., Clausen B., Tomé C.N., Wu P.D., 2013a. Studying the effect of stress relaxation and creep on lattice strain evolution of stainless steel under tension. Acta Materialia 61, 1179-1188.

Wang H., Wu P.D., Wang J., 2013b. Modeling inelastic behavior of magnesium alloys during cyclic loading-unloading. International Journal of Plasticity 47, 49-64.

Wang H., Wu P.D., Wang J., Tomé C.N., 2013c. A crystal plasticity model for hexagonal close packed crystals including twinning and de-twinning mechanisms. International Journal of Plasticity 49, 36-52.

Wang H., Wu P.D., Wang J., 2015a. Numerical assessment of the role of slip and twinning in magnesium alloy AZ31B during loading path reversal. Metallurgical and Materials Transactions A 46, 3079-3090.

Wang H., Wu P.D., Wang J., 2015b. Modelling the role of slips and twins in magnesium alloys under cyclic shear. Computational Materials Science 96, 214-218.

Wang H., Clausen B., Capolungo L., Beyerlein I.J., Wang J., Tomé C.N., 2016a. Stress and strain relaxation in magnesium AZ31 rolled plate: In-situ neutron measurement and elastic viscoplastic polycrystal modeling. International Journal of Plasticity 79, 275-292.

Wang H., Lee S.Y., Gharghouri M.A., Wu P.D., 2016b. Deformation behavior of Mg-8.5wt.%Al alloy under reverse loading investigated by in-situ neutron diffraction and elastic viscoplastic self-consistent modeling. Acta Materialia 107, 404-414.

Wang H., Jeong Y., Clausen B., Liu Y., McCabe R.J., Barlat F., Tomé C.N., 2016c. Effect of martensitic phase transformation on the behavior of 304 austenitic stainless steel under tension. Materials Science and Engineering: A 649, 174-183.

Wang H., Capolungo L., Clausen B., Tomé C.N., 2017. A crystal plasticity model based on transition state theory. International Journal of Plasticity 93, 251-268.

Watanabe H., Ishikawa K., 2009. Effect of texture on high temperature deformation behavior at high strain rates in a Mg-3Al-1Zn alloy. Materials Science and Engineering A523, 304-311.

Wu, P.D., Neale, K.W., Van der Giessen, E., 1996. Simulation of the behaviour of FCC polycrystals during reversed torsion. International Journal of Plasticity 12, 1199-1219.

Wu P.D., Neale, K.W., Van der Giessen, E., 1997. On crystal plasticity FLD analysis. Proceedings of the Royal Society A453, 1831-1848.

Wu W., Qiao H., An K., Guo X.Q., Wu P.D., Liaw P.K., 2014. Investigation of deformation dynamics in a wrought magnesium alloy. International. Journal of Plasticity 62, 105-120.

Xie Q.J., Zhu Z.W., Kang G.Z., Yu C., 2016. Crystal plasticity-based impact dynamic constitutive model of magnesium alloy. International Journal of Mechanical Sciences 119,107-113.

Zheng Z. B, Balint D. S., Dunne F. P. E., 2016. Rate sensitivity in discrete dislocation plasticity in hexagonal close packed crystals, Acta Materialia 107,17-26.

Highlights:

1) Numerical stability of EVPSC model when treating multiple/small SRSs is enhanced.
2) Rate sensitivity of Mg alloys can be better described by using multiple SRSs.
3) SRSs are obtained for basal, prismatic, pyramidal slip and extension twinning.
4) Compact slip systems corresponds to low SRS; twinning is rate insensitive.
5) The SRSs are validated by internal elastic strain and a rate related experiment.